

# Alkyl-thiol Langmuir Films on the Surface of Liquid Mercury

H. Kraack,<sup>†,§</sup> L. Tamam,<sup>†</sup> E. Sloutskin,<sup>†</sup> M. Deutsch,<sup>†</sup> and B. M. Ocko<sup>\*,‡</sup>

Department of Physics, Bar-Ilan University, Ramat-Gan 52900, Israel, and Department of Condensed Matter Physics and Materials Science, Brookhaven National Laboratory, Upton, New York 11973

Received January 17, 2007. In Final Form: April 4, 2007

The coverage dependent phase behavior of monolayers of alkyl thiols ( $\text{CH}_3(\text{CH}_2)_{n-1}\text{SH}$ , denoted as  $C_n\text{SH}$ ) on mercury was studied for chain lengths  $9 \leq n \leq 22$ , using surface tensiometry and surface-specific X-ray scattering methods. At low coverage, a disordered single layer of surface-parallel molecules is found for all  $n$ . At high coverage, a monolayer of standing-up molecules is formed, exhibiting well-ordered phases, the structure of which is  $n$ - and coverage-dependent. The molecular chains pack in a centered rectangular unit cell, with an  $\sim 27^\circ$  tilt from the surface normal toward nearest neighbors. The strong sulfur–mercury bond induces a noncentered unit cell for the headgroups, incorporating one mercury atom per two thiol molecules. The small but significant differences in structure of these films on gold and on mercury are discussed and assigned to the different structure of the subphase: long-range-ordered crystal for gold and short-range-ordered liquid for mercury.

## I. Introduction

Solid- and liquid-supported monolayers of organic films have been studied intensively for more than a century. This interest is driven by the need to elucidate the basic physics of two-dimensional systems and its dependence on different types of molecular interactions and by the importance of these films for a variety of potential technological applications like, e.g., wetting and corrosion control of solid surfaces<sup>1,2</sup> and nanoscale construction and self-assembly of devices with desirable electrical and/or optical properties.<sup>3–6</sup> The first modern studies of such films started in the late 19th century with Langmuir films of fatty acid amphiphiles on water.<sup>7,8</sup> In such water-supported films the molecules align roughly perpendicular to the water surface with their hydrophilic headgroup residing on the surface and their hydrophobic tail pointing along, or close to, the surface normal. The phases and structures of Langmuir monolayers (LMs) can be tuned by varying the coverage, the temperature, and the chain length. A measure of universality of the phase diagram in these variables was demonstrated for fatty acids.<sup>9</sup> The phases and their different structure, symmetry and order, and the phase transitions between the different phases were reviewed by Kaganer et al.<sup>10</sup> A Landau theory describing the phase diagram of these systems has also been published.<sup>10</sup>

A related field of research deals with organic films on *solid* substrates, mostly metals or semiconductors. Detailed reviews on these self-assembled monolayers (SAMs) were published by Schreiber<sup>11</sup> and Ulman.<sup>12,13</sup> The most-studied SAMs are those

of alkyl thiols on the Au(111) surface. SAMs are fundamentally different from liquid-supported LMs because of the different interactions between the overlayers' molecules and the subphase. For the solid-supported SAMs these interactions lead, more often than not, to the order in the SAM being induced epitaxially by the crystalline structure of the substrate. No such order exists in a laterally unstructured liquid subphase. This tendency toward epitaxy is further enhanced by the fact that SAMs are normally strongly chemisorbed to the solid substrate. A particularly prominent example is the  $\sim 128$  kJ/mol bond of the sulfur atom of thiol SAMs to the Au(111) substrate,<sup>14</sup> as compared to the  $\sim 15$  kJ/mol hydrogen bond of an acidic headgroup to the aqueous subphase in a typical water-supported fatty acid Langmuir monolayer. Thus, the headgroup–substrate interaction often becomes dominant in SAMs to the extent that it determines the molecular structure of the film. By contrast, for Langmuir films on water the chain–chain Van der Waals interaction is more dominant in determining the in-plane structure.

There are several reasons for the great interest in thiols on gold over the past three decades. The strong chemisorption of the thiol headgroup onto the gold surface renders these SAMs reasonably robust, which is a very desirable quality for device applications. The robustness allows these films to be studied under a broad range of environments and conditions with a variety of experimental techniques, some of which are potentially destructive. Moreover, thiol films on gold are easier to prepare reproducibly and in an almost defect-free state, as compared to other films, e.g., trichlorosilanes on the native silicon oxide, which forms at the surface of silicon<sup>15</sup> in the presence of residual water. Finally, the use of alkyl spacers and different functional endgroups allows one to tune easily the properties of the free surface of these SAMs. Changing, for example, between a hydrophobic and a hydrophilic endgroup modifies the wetting behavior of the film-covered substrate.<sup>1</sup> Chemical and geometrical

\* To whom correspondence should be addressed. E-mail: ocko@bnl.gov.

<sup>†</sup> Bar-Ilan University.

<sup>‡</sup> Brookhaven National Laboratory.

<sup>§</sup> Present address: Infineon Technologies, Villach, Austria.

(1) Bain, C. D.; Whitesides, G. M. *Angew. Chem., Int. Ed. Engl.* **1989**, *28*, 506.

(2) Scherer, J.; Vogt, M. R.; Magnussen, O. M.; Behm, R. *J. Langmuir* **1997**, *13*, 7045.

(3) Campbell, I. H.; et al. *Appl. Phys. Lett.* **1997**, *71*, 3528.

(4) Jortner, J.; Ratner, M. Eds; Balckwell, Oxford, 1997; Samori, P.; Rabe, J. P. *J. Phys. Condens. Matter* **2002**, *14*, 9955.

(5) Cahen, D.; Hodes, G. *Adv. Mater.* **2002**, *14*, 789.

(6) Venkataraman, L.; Klare, J. E.; Nuckolls, C.; Hybersten, M. S.; Steigerwald, M. L. *Nature* **2006**, *442*, 904.

(7) Pockels, A. *Nature* **1891**, *43*, 437.

(8) Rayleigh, L. *Phil. Mag.* **1899**, *48*, 321.

(9) Peterson, I. R.; et al. *Langmuir* **1992**, *8*, 2995.

(10) Kaganer, V. M.; et al. *Rev. Mod. Phys.* **1999**, *71*, 779.

(11) Schreiber, F. *Prog. Surf. Sci.* **2000**, *65*, 151.

(12) Ulman, A. *An Introduction to Ultrathin Organic Films: From Langmuir-Blodgett to Self-Assembly*; Academic Press: Boston, 1991.

(13) Ulman, A., Ed. *Thin Films: Self-Assembled Monolayers of Thiols*; Academic Press: San Diego, 1998.

(14) Lavrich, D. J.; Wetterer, S. M.; Bernasek, S. L.; Scoles, G. *J. Phys. Chem. B* **1998**, *102*, 3456.

(15) Maoz, R.; Sagiv, J. *J. Colloid Interface Sci.* **1984**, *100*, 465. Maoz, R.; Matlis, S.; DiMasi, E.; Ocko, B. M.; Sagiv, J. *Nature* **1996**, *384*, 150.

patterning of the free surface is also possible by using molecules with different endgroups.<sup>16</sup>

Two distinct types of structures were found for SAMs of thiols on gold. At low surface coverage, thiols form a so-called striped phase of molecules lying down on the gold surface. These phases are commensurate with the periodicity of the Au(111) surface, having a stripe width of 5.0 Å, which is  $\sqrt{3}$  times the nearest-neighbor distance between gold atoms on the surface. The stripe length depends on the molecule's length, but it is also commensurate, albeit at a high order, with the underlying gold substrate. At a high coverage, phases of standing-up molecules on the gold surface are found which have an increasingly more complicated structure as the symmetry favored by the chains and that favored by the headgroup deviate from each other. The chains form a commensurate hexagonal ( $\sqrt{3} \times \sqrt{3}$ )R30° structure with a nearest-neighbor distance of 5.0 Å and with the chains tilted  $\sim 32^\circ$  away from the surface normal in a nonsymmetric azimuthal direction. The deviation of the azimuthal angle from the next-nearest neighbor direction depends on the chain length of the molecule.<sup>11</sup> The thiol headgroups of two neighboring molecules are pairwise closer to each other than their respective chains and may bond to form a disulfide.<sup>17</sup> The thiol adlayer forms a  $c(4 \times 2)$  super-cell, manifested in the appearance of additional peaks in the diffraction pattern.<sup>17</sup> An alternative explanation for this symmetry is the distortion of the top-layer of gold atoms.<sup>18</sup> Indeed, for methylthiols on the Au(111) surface, a significant distortion of the top atomic layer of the gold substrate has been reported.<sup>19</sup>

Thiols on liquid mercury, the subject of the present study, is an intriguing intermediate case between a LM on an aqueous subphase and a SAM supported on a single-crystal metal substrate. The liquid mercury subphase is similar to water in presenting to the monolayer a liquid, disordered surface with mobile molecules lacking intrinsic crystalline structure and being atomically smooth. At the same time, it has the same strong interactions with organic molecules, in particular thiols, as other metallic substrates, in particular gold. Mercury was shown to be a subphase of choice for the nucleation of 2D protein crystallite<sup>20</sup> and for molecular "Tinkertoy"-like self-assembly of supramolecular networks and structures from star-shaped and other types of monomers.<sup>21</sup> Mercury electrodes have been utilized for electron-transfer studies through different classes of molecules, including alkyl thiols,<sup>22–28</sup> in which the second electrode is typically a silicon or a solid metal surface.

The present investigations build on earlier X-ray scattering studies of the mercury surface.<sup>29–31</sup> The first Ångström-resolution determination of surface structure of the bare mercury surface was reported a decade ago,<sup>30</sup> where a quasi-Bragg layering peak was observed. Subsequent studies of the mercury surface discovered non capillary-wave-like temperature-dependent surface fluctuations<sup>31</sup> and surface segregation in mercury/gold alloys.<sup>32</sup> The first reported X-ray scattering investigation of organic molecular layers on the mercury surface was for stearic acid at a high surface coverage.<sup>33</sup> In that study an ordered monolayer structure was proposed on the basis of grazing incident angle diffraction studies alone. Subsequent X-ray reflectivity studies of dense monolayers showed that fatty acid<sup>34</sup> and alkylthiol molecules<sup>35</sup> stand up at the mercury surface. In the past several years, extensive X-ray scattering studies, using both X-ray reflectivity and grazing incident angle diffraction methods, of different organic Langmuir films on the mercury surface have been carried out by our group<sup>35–42</sup> and by Harzallah and Cortes.<sup>43</sup> These studies revealed a plethora of new phases and phase transitions, including several single-layers and multilayers of surface-parallel-oriented molecules not observed on aqueous subphases. Transitions from phases of surface-parallel to surface-normal molecules,<sup>37–41</sup> and from flat-lying to side-lying molecules<sup>36</sup> were also found.

Several molecular-resolution studies of the structure of LMs of thiol molecules, mostly alkyl-thiols, on the mercury surface have been published previously.<sup>35,42,44,45</sup> The first studies, carried out a decade ago in the absence of precise coverage control, revealed a monolayer of densely packed standing-up molecules.<sup>35</sup> The absence of in-plane order in those studies was likely due to beam damage, caused by the intense, focused synchrotron radiation at the ESRF, where that study was carried out.<sup>35,45</sup> The intensity there was higher by an order of magnitude or more than that used in the present study. For higher-than-monolayer coverages, multilayers exhibiting surface-parallel order were found.<sup>44</sup> Studies of mercaptobiphenyl thiol molecules, terminated by either methyl or perfluoromethyl groups, on the mercury surface revealed that the low-coverage lying-down, disordered phases transform at high coverage into an in-plane ordered structure of standing-up molecules, the areal densities of which were smaller than those for the same molecules on Au(111).<sup>42</sup>

(16) Nam, Y.; Chang, J. C.; Wheeler, B. C.; Brewer, G. J. *IEEE Trans. Biomed. Eng.* **2004**, *51*, 158. Brockman, J. M.; Frutos, A. G.; Corn, R. M. *J. Am. Chem. Soc.* **1999**, *121*, 8044. Liu, M. Z.; Amro, N. A.; Chow, C. S.; Liu, Y. G. *Nano Lett.* **2002**, *2*, 863.

(17) Fenter, P.; Eberhardt, A.; Eisenberger, P. *Science* **1994**, *266*, 1216.

(18) Torrelles, X.; Barrena, E.; Munuera, C.; Rius, J.; Ferrer, S.; Ocal, C. *Langmuir* **2004**, *20*, 9396.

(19) Mazzarello, R.; Cossaro, A.; Verdini, A.; Rousseau, R.; Casalis, L.; Danisman, M. F.; Floreano, L.; Scandolo, S.; Morgante, A.; Scoles, G. *Phys. Rev. Lett.* **2007**, *98*, 016102.

(20) Fojta, M.; Vetterl, V.; Tomschik, M.; Jelen, F.; Nielsen, P.; Wang, J.; Palecek, E. *Biophys. J.* **1997**, *72*, 2285. Dimitrov, A. S.; Yoshimura, H.; Nagayama, K. *Langmuir* **1995**, *11*, 3937. Nagayama, K.; Takeda, S.; Endo, S.; Yoshimura, H. *Jpn. J. Appl. Phys.* **1995**, *34*, 3947.

(21) Varaksa, N.; Pospisil, L.; Magnera, T. F.; Michl, J. *Proc. Nat. Acad. Sci.* **2002**, *99*, 5012. Michl, J.; Magnera, F. *Proc. Nat. Acad. Sci.* **2002**, *99*, 4788.

(22) Rampi, M. A.; Whitesides, G. M. *Chem. Phys.* **2002**, *281*, 373.

(23) Slowinski, K.; Chamberlain, R. V.; Miller, C. J.; Majda, M. *J. Am. Chem. Soc.* **1997**, *119*, 11910.

(24) Slowinski, K.; Fong, H. K. Y.; Majda, M. *J. Am. Chem. Soc.* **1999**, *120*, 7257. Slowinski, K.; Majda, M. *J. Electroanal. Chem.* **2000**, *491*, 139.

(25) Salomon, A.; Cahen, D.; Lindsay, S.; Tomfohr, J.; Engelkes, V. B.; Frisbie, C. D. *Adv. Mater.* **2003**, *15*, 1881.

(26) Salomon, A.; Boecking, T.; Chan, C. K.; Amy, F.; Girshkevitz, O.; Cahen, D.; Kahn, A. *Phys. Rev. Lett.* **2005**, *95*, 266807.

(27) Muskal, N.; Mandler, D. *Electrochim. Acta* **1999**, *45*, 537.

(28) Neshet, G.; et al. *J. Phys. Chem. B* **2006**, *110*, 14363.

(29) Barton, S. W.; et al. *Nature* **1986**, *321*, 685. Lu, B. C.; Rice, S. A. *J. Chem. Phys.* **1978**, *68*, 5558. Bosio, L.; Oumezine, M. *Chem. Phys.* **1984**, *80*, 959. Bosio, L.; et al. *J. Electrochem. Soc.* **1992**, *139*, 2110.

(30) Magnussen, O. M.; et al. *Phys. Rev. Lett.* **1995**, *74*, 4444.

(31) DiMasi, E.; Tostmann, H.; Ocko, B. M.; Pershan, P. S.; Deutsch, M. *Phys. Rev. B* **1998**, *58*, 13419.

(32) DiMasi, E.; Tostmann, H.; Ocko, B. M.; Pershan, P. S.; Deutsch, M. *J. Phys. Chem. C* **1999**, *103*, 9952.

(33) Barton, S. W.; Thomas, B. N.; Flom, E. B.; Novak, F.; Rice, S. A. *Langmuir* **1988**, *4*, 233.

(34) Harzallah, B.; Bosio, L.; Cortes, R.; Erraffi, N. *J. Chim. Phys.* **1996**, *93*, 1202.

(35) Magnussen, O. M.; Ocko, B. M.; Deutsch, M.; Regan, M. J.; Pershan, P. S.; Berman, L. E.; Abernathy, D.; Legrand, J. F.; Grübel, G. *Nature* **1996**, *384*, 250.

(36) Tamam, L.; Kraack, H.; Sloutskin, E.; Ocko, B. M.; Pershan, P. S.; Ofer, E.; Deutsch, M. *J. Phys. Chem. C* **2007**, *111*, 2573; 2580.

(37) Kraack, H.; Deutsch, M.; Ocko, B. M.; Pershan, P. S. *Nucl. Inst. Meth. Phys. Res. B* **2003**, *200*, 363.

(38) Kraack, H.; Ocko, B. M.; Pershan, P. S.; Sloutskin, E.; Deutsch, M. *J. Chem. Phys.* **2003**, *119*, 10339.

(39) Kraack, H.; Ocko, B. M.; Pershan, P. S.; Sloutskin, E.; Tamam, L.; Deutsch, M. *Langmuir* **2004**, *20*, 5375; *ibid.* **2004**, *20*, 5386.

(40) Kraack, H.; Ocko, B. M.; Pershan, P. S.; Sloutskin, E.; Deutsch, M. *Science* **2002**, *298*, 1404.

(41) Kraack, H. Ph.D. Thesis, Bar Ilan University, 2004.

(42) Tamam, L.; Kraack, H.; Sloutskin, E.; Ocko, B. M.; Pershan, P. S.; Ulman, A.; Deutsch, M. *J. Phys. Chem. B* **2005**, *109*, 12534.

(43) Harzallah, B.; Cortes, R. *J. Phys. IV* **2004**, *118*, 221.

(44) Deutsch, M.; et al. in ref 13.

(45) Ocko, B. M.; Kraack, H.; Pershan, P. S.; Sloutskin, E.; Tamam, L.; Deutsch, M. *Phys. Rev. Lett.* **2005**, *94*, 017802.

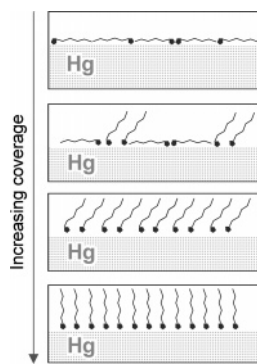


**Figure 1.** Schematic view of the structure of a Langmuir film of alkyl thiols on the mercury surface. A single layer of lying-down molecules is observed at the lowest coverage. At the highest coverage a standing-up phase is observed which is either untilted or tilted. At intermediate coverages a coexistence between lying-down and standing-up phases is observed.

Recently structural studies of alkyl-thiol molecules on the mercury surface have been extended to the buried interface between silicon and mercury by using high-energy X-ray reflectivity.<sup>46</sup> At this buried interface, the C18SH high-coverage monolayer forms a densely packed, standing-up phase, a structure consistent with that formed at the free mercury surface.

In this paper we present a detailed study of the structure and thermodynamics of Langmuir films of several different chain-length alkyl-thiols on the free surface of mercury as a function of coverage and temperature. We expand here on a previous letter, which focused on octadecanethiol.<sup>45</sup> In the present investigations, the thermodynamics were studied using surface-tension measurements while the structure was studied using surface-specific X-ray methods including X-ray reflectivity, grazing incidence diffraction, and Bragg-rod measurements. A schematic view of the various phases found is shown in Figure 1. With increasing coverage, we observe first a single layer of surface-parallel-oriented molecules, i.e., a lying-down phase. At the highest coverages, we find standing-up phases where the molecules are oriented along, or tilted from, the surface normal. The monolayers of the surface normal molecules, both tilted and untilted, were found to be ordered in-plane. Further, in the tilted phase, the unit cell is centered for the chains and noncentered for the headgroups. These results suggest that the thiol headgroups associate in pairs with a single Hg atom and that the bonds form long-range orientational order. At intermediate coverages, we find a region where the standing-up and lying-down phases coexist. A detailed description of these phases, including their in-plane structure, is given below.

## II. Experimental Section

As the experimental details have been discussed in previous publications,<sup>38,39,41</sup> we provide here only a very short description.

A specially designed Langmuir trough, suitable for simultaneous surface tension and X-ray studies, was used for the experiments. It consisted of an inner KelF trough, enclosed in a hermetically sealable aluminum enclosure. The enclosure was filled with either helium or nitrogen to reduce surface contamination of the mercury and beam damage to the LMs. The temperature of the mercury was controlled by a water circulation system to  $\pm 0.2$  °C.

The surface tension was measured by the Wilhelmy plate method,<sup>47</sup> using a mercury-amalgamated platinum plate. The plate was hung from a leaf spring, the deviation of which from the equilibrium

position (which is proportional to the surface tension) was measured by a linear variable differential transformer (LVDT).

Mercury was purchased from Merck Co. (triple distilled, 99.999% pure) and from Bethlehem Apparatus Co. (quadruple distilled 99.99995% pure). Alkyl thiols with lengths  $n \leq 20$  were purchased from Fluka or Aldrich and were at least 97% pure. The C22SH was a gift from Prof. C. E. D. Chidsey (Stanford University). All materials were used as received without further purification. No differences in the results presented here were found when using mercury or thiols from different manufacturers or purities. Standard spreading solutions were prepared with molarities in the range of  $3-8 \times 10^{-4}$  using HPLC grade, 99.9% pure chloroform (Aldrich). Deposition of films was done by a micropipette through a sealable opening in the top plate of the trough's enclosure.

## III. Measurement Methods

**A. Surface Pressure–Molecular Area Isotherms.** The surface pressure,  $\pi = \sigma_0 - \sigma$ , is the difference between the surface tension of the uncovered, ( $\sigma_0$ ), and film-covered, ( $\sigma$ ), mercury. It varies with surface coverage, given by the area per molecule,  $A$ , as calculated from the trough area and the number of deposited molecules, through the dependence of  $\sigma$  on  $A$ .<sup>47</sup> Features in the  $\pi(A)$  isotherm provide hints for the molecular structure of, and phase transitions in, the Langmuir film.

Since a well-sealing barrier is notoriously difficult to construct for mercury,<sup>48</sup> the coverage was increased not by barrier compression, as done conventionally, but rather by a stepwise addition of the standard solution, employing a calibrated micropipette. In each step material was added only after a full pressure equilibration of the previous step was reached.<sup>38</sup>

**B. X-ray Measurements.** The surface specific X-ray measurements were carried out using the Harvard/BNL liquid surface spectrometer at beamline X22B, NSLS, Brookhaven National Laboratory, with wavelengths of  $\lambda = 1.53-1.58$  Å. The trough was supported on an active vibration isolation unit, mounted on the spectrometer.<sup>49</sup> This arrangement was demonstrated in previous measurements<sup>35,38</sup> to minimize vibrational pickup from the environment, in part a cause of the limited measurement range explored in early studies of the surface structure of mercury.<sup>29</sup>

A detailed description of the X-ray measurement methods used is available in the literature<sup>10,50,51</sup> and will not be repeated here. We have carried out X-ray reflectivity (XR) measurements, where we measure the fraction of the incident intensity reflected specularly from the surface,  $R(q_z)$ , as a function of the surface-normal wave vector transfer,  $q_z = (2\pi/\lambda)(\sin \alpha + \sin \beta)$ , which is a function of the incidence angle,  $\alpha$ , and the detection angle,  $\beta$ . For XR,  $\alpha = \beta$ . XR yields information on the surface-normal structure of the Langmuir film such as its surface-normal electron density profile, its layer thickness, and its surface roughness. The in-plane order was investigated by grazing incidence diffraction (GID), where the diffracted intensity is measured as a function of the surface parallel wave vector transfer  $q_{||} = (2\pi/\lambda)\sqrt{\cos^2 \alpha + \cos^2 \beta - 2\cos \alpha \cos \beta \cos 2\theta}$ , with  $2\theta$  being the surface-parallel angular offset of the detector from the plane of reflection. The XR measurements employed a NaI point detector, while the GID was measured using Soller slits and a surface-normal-aligned position-sensitive detector (PSD). The PSD allows the measurement, simultaneously with the GID, of full Bragg rods (BR), which are the  $q_z$  distributions of the intensity at the  $2\theta$  positions where the GID peaks are observed. The BR yields information on the LM's thickness, the magnitude of the molecular tilt, and its azimuthal direction. To minimize beam damage, exposure times of the sample were kept to

(48) Smith, T. *Adv. Colloid Interface Sci.* **1972**, *3*, 161.

(49) Braslau, A.; Pershan, P. S.; Swislow, G.; Ocko, B. M.; Als-Nielsen, J. *Phys. Rev. A* **1988**, *38*, 2457.

(50) Als-Nielsen, J.; Christensen, F.; Pershan, P. S. *Phys. Rev. Lett.* **1982**, *48*, 1107; Pershan, P. S.; Als-Nielsen, J. *Phys. Rev. Lett.* **1984**, *52*, 759.

(51) Als-Nielsen, J.; McMorrow, D. *Elements of Modern X-Ray Physics*; Wiley: New-York, 2001. Deutsch, M.; Ocko, B. M. Ocko In *Encyclopedia of Applied Physics*; Trigg, G. L., Ed.; VCH: New York, 1998; Vol. 23, p 479.

(46) Lefenfeld, M.; Baumert, J.; Sloutskin, E.; Kuzmenko, I.; Pershan, P.; Deutsch, M.; Nuckolls, C.; Ocko, B. M. *Proc. Nat. Acad. Sci.* **2006**, *103*, 2541.

(47) Gaines, G. L. *Insoluble Monolayers at Liquid-Gas Interfaces*; Wiley-Interscience: New York, 1966.

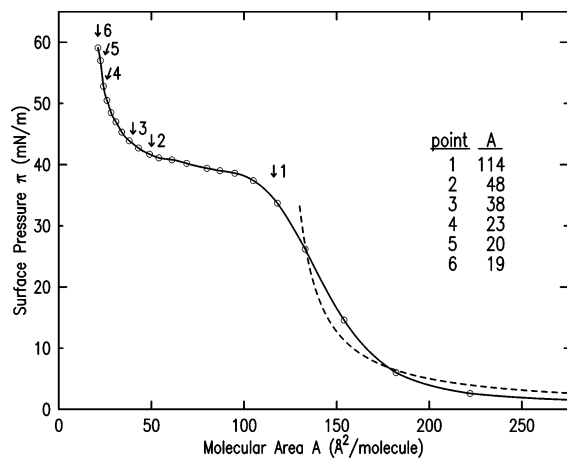


**Figure 2.**  $\pi(A)$  isotherm for C18SH (solid line + points) and a fit of the higher- $A$  part of the isotherm by the Volmer equation (dashed line) of an ideal two-dimensional gas of finite-size molecules. The table lists coverages, indicated by numbered arrows, for which X-ray reflectivity curves were measured.

the necessary minimum by using an automated shutter upstream of the trough. It was opened only during photon counting.

#### IV. Results and Discussion

We will first show the  $\pi(A)$  isotherm results and then present the X-ray data. This will be followed by a discussion of the dependence of the results on chain length and of the phase diagram constructed from all data available. The results will then be discussed within the context of the recently determined phase diagrams of fatty acids, alcohols, and alkanes on mercury.<sup>38,39</sup> Finally, a comparison with SAMs of alkyl thiols on gold will be given.

**A. Surface Pressure–Area Isotherms.** Figure 2 shows the isotherm of C18SH. The measured points (circles) are connected by a smoothed solid line. At low coverage,  $A \geq 180 \text{ \AA}^2/\text{molecule}$ , the surface pressure does not change significantly with  $A$  and stays below  $\pi \leq 5 \text{ mN/m}$ . For  $110 \lesssim A \lesssim 180 \text{ \AA}^2/\text{molecule}$ ,  $\pi$  increases strongly and reaches  $\pi \approx 40 \text{ mN/m}$  at a molecular area of  $A \approx 110 \text{ \AA}^2/\text{molecule}$ . The isotherm in this range can be described by the Volmer equation, an ideal gas law in two dimensions:  $\pi(A - A_1) = kT$ .  $A_1$  is the exclusion area due to the finite size of the molecule. Although the fit (dashed line) is not perfect, the resultant exclusion area,  $A_1 = 118 \text{ \AA}^2/\text{molecule}$ , is very close to the expected geometrical area occupied by a single C18SH molecule lying flat on the mercury surface, in line with the long-standing prediction of Langmuir<sup>52</sup> for LMs on water. The value of  $A_1$  is also very close to those measured for LMs of other chain molecules of the same length on mercury.<sup>38,39</sup> Reducing  $A$  below  $A_1$  leaves  $\pi$  almost constant over a fairly large  $A$  range down to  $A \approx 40 \text{ \AA}^2/\text{molecule}$ . Previous studies on alcohols and fatty acid Langmuir films on mercury<sup>37–40</sup> and our X-ray measurements discussed below indicate that this plateau results from a coexistence between phases of lying-down and standing-up molecules. Decreasing  $A$  below  $\sim 40 \text{ \AA}^2/\text{molecule}$  results in a sharp increase in the surface pressure, reaching  $60 \text{ mN/m}$  at  $A = 19 \text{ \AA}^2/\text{molecule}$ . The rise obviously starts when the islands of standing-up molecules, which are surrounded by a “sea” of the lying-down phase,<sup>39</sup> grow to a point where they become close enough to each other (perhaps touching) to require a significant pressure increase for further compression. This rise in  $\pi$  at low  $A$  is much stronger than that observed for Langmuir films of fatty acids and alcohols on mercury.<sup>39,40</sup>

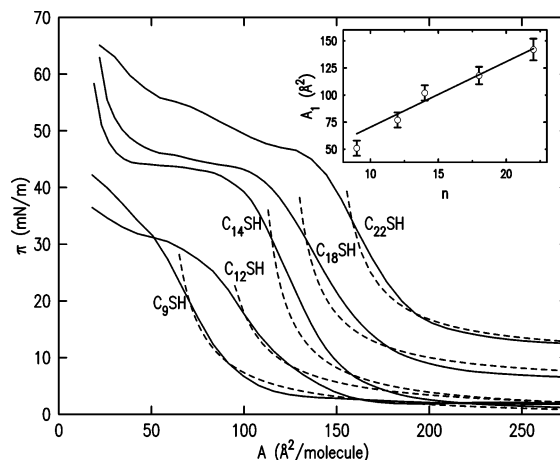


**Figure 3.** Isotherms of alkyl thiols for chain lengths  $9 \leq n \leq 22$  (solid lines) and fits by the Volmer equation (dashed lines). The isotherms of C18SH and C22SH are shifted up for clarity by  $\pi = 5$  and  $10 \text{ mN/m}$ , respectively. The inset shows a linear fit to the exclusion areas  $A_1$ , obtained from the Volmer equation fits, for the different chain lengths,  $n$ .

The  $\pi(A)$  isotherms measured at  $T = 23 \text{ }^\circ\text{C}$  for thiols of chain lengths  $9 \leq n \leq 22$  are shown in Figure 3. The isotherms for C14SH and C18SH are very similar in shape. They both show a sharp rise at the molecular area of a lying-down molecule followed by a flat plateau and again a sharp rise at a high coverage between  $35$  and  $20 \text{ \AA}^2/\text{molecule}$ . The isotherms for C22SH and C12SH also show a clear rise at areas corresponding to the molecular area of a lying-down molecule. The plateau for both of these isotherms is less horizontal than those of C14SH and C18SH, reflecting possible structural changes in one or both of the coexisting phase. This could be, for example, a variation with  $A$  of the molecular tilt or of the unit cell dimensions. The exclusion areas  $A_1$  obtained from fits by the Volmer equation are shown in the inset of Figure 3.  $A_1$  increases linearly with the chain length of the molecules:  $A_1 = (6.04 \pm 0.3)n + (10 \pm 6) \text{ \AA}^2/\text{molecule}$ . Dividing the slope by the mean projected C–C distance on the molecular long axis yields a chain–chain spacing of  $6.04 \text{ \AA}^2/1.27 \text{ \AA} = 4.76 \text{ \AA}$ . This distance is very close to the in-plane lattice constant of hexagonally packed alkanes ( $22 \leq n \leq 26$ ) in the rotator  $R_{II}$  phase, which has a chain–chain spacing of  $4.77 \pm 0.01 \text{ \AA}$ .<sup>53</sup>

The shape of the isotherm of C9SH is different from the others. It does not show a clear plateau but just a slight change in slope at some intermediate  $A$  close to the expected molecular area of a lying-down C9SH molecule. The inset also shows that the Volmer-fit-derived exclusion area for C9SH falls below the linear behavior of the other thiols. Both the absence of a clear plateau and the too-small exclusion area for C9SH may indicate that the molecules of C9SH start to stand up before a single layer of lying-down molecules is completed, as was observed also for short-chain alcohol and fatty acid molecules on mercury.<sup>37,38,40</sup> The data derived from the isotherms are summarized in Table 1.

In contrast with other chain molecules, we do not observe the formation of multiple plateaus in the isotherms. This indicates the absence of multilayers of lying-down molecules and thus the formation of only a single layer of lying-down molecules. This behavior is similar to that of SAMs of thiols on gold and is most likely caused by the strong chemisorption of the thiol headgroup to the mercury surface, so that the molecules require only a

(52) Langmuir, I. *J. Am. Chem. Soc.* **1932**, *54*, 2798.

(53) Sirota, E. B.; King, H. E., Jr.; Singer, D. M.; Shao, H. H. *J. Chem. Phys.* **1992**, *5809*.

**Table 1. Fitted Exclusion Areas  $A_1$ , with the Experimental Uncertainty Given in Parenthesis<sup>a</sup>**

$n$	$A_1$ $\text{\AA}^2/\text{molecule}$	$\pi_1$ mN/m	$\pi_c$ mN/m
9	51(7)	27(6)	41(4)
12	77(7)	29(5)	37(5)
14	102(7)	41(3)	61(4)
18	118(8)	38(4)	58(4)
22	142(10)	37(4)	57(6)

<sup>a</sup> The surface pressures of the plateau,  $\pi_1$ , and the collapse pressures,  $\pi_c$ , are also listed.

moderate surface pressure to cause them to stand up. Another difference from other chain molecules on mercury is the stronger increase in the surface pressure toward the low- $A$  end of the isotherm. For thiols we observe a difference of  $\pi_c - \pi_1 \approx 20$  mN/m between the plateau and the collapse pressures whereas for fatty acids and alcohols the observed pressure difference is 3–10 mN/m.<sup>39,40</sup> This larger pressure difference for the thiols is also likely to result from the much stronger binding between the thiol headgroup and mercury as compared with the non-thiol molecules.

Finally, we note that the Volmer equation assumes a hard-sphere interaction between the monolayer's molecules. More realistic intermolecular interactions may be accommodated by using one of the several modifications of the Volmer equation available in the literature.<sup>54</sup> This should improve the fit to the  $A > A_1$  regions of the isotherms in Figures 2 and 3. A preliminary check indicates, however, that the resultant changes in the  $A_1$  values would be minor. More reliable fits would require measuring more, and more accurate,  $\pi(A)$  values in the large- $A$  region.

**B. X-ray Measurements.** Here we describe the results obtained from X-ray measurements on Langmuir films of C14SH, C18SH, and C22SH on mercury at selected points on their respective isotherms. We focus first on C18SH, for which the most extensive data set was measured.

**1. C18SH: Reflectivity.** Figure 4 shows a set of reflectivities measured for C18SH at the indicated coverages for  $T = 26$  °C. These coverages are also marked by arrows on the isotherm in Figure 2. Figure 4a shows the measured reflectivities divided by the Fresnel reflectivity of an ideal flat mercury surface (open circles) along with a fit by a slab model (lines). The corresponding electron density profiles derived from the fit are shown in Figure 4b. The slab model consists of a total of eight slabs. Of these, one or two are used to model the thiols, depending on whether the molecules stand up or lie down. The remaining slabs are used to represent the electron density profile of the mercury below the surface.<sup>30</sup> The close-packed alkyl chains, both standing up and lying down, are modeled by a single slab of density  $\rho = 0.30$  electrons/ $\text{\AA}^3$  and a variable thickness. For the standing-up phases, an additional layer, of a fixed electron density of 0.7 electrons/ $\text{\AA}^3$  and a fixed thickness of 2.5  $\text{\AA}$  describe the thiol headgroups' region. As pointed out in refs 38–40, for thin layers the density and thickness fit parameters are coupled and a refinement of both, along with other parameters, is unreliable. Thus, the procedure used is to conduct a series of preliminary fits with different combinations of fixed and free parameters and to obtain the combination that provides the best overall fit to several related XR curves. These values are kept fixed in subsequent fits. Note that if this layer included only the sulfur headgroups a density of  $\sim 0.3$  electrons/ $\text{\AA}^3$  should have ensued. The higher density obtained in the preliminary fits supports the conclusion that the

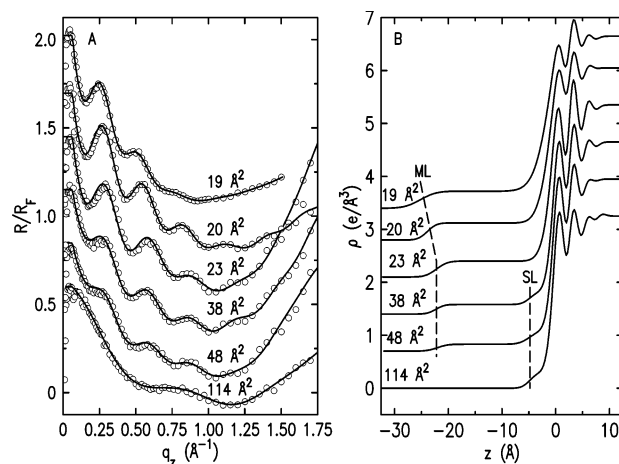


**Figure 4.** (a) X-ray reflectivities (open circles), measured at  $T = 26$  °C, and slab model fits (lines) for C18SH on mercury at the indicated coverages. (b) The surface-normal electron density profiles corresponding to the fits. From bottom to top, the XR curves show a single layer (SL) of lying-down molecules (114  $\text{\AA}^2$ ), a coexistence between standing-up monolayer (ML) and lying-down SL phases (38 and 48  $\text{\AA}^2$ ), and pure standing-up ML phases, which are tilted for intermediate coverages (23 and 20  $\text{\AA}^2$ ) and untilted for the highest coverage shown, 19  $\text{\AA}^2$ .

**Table 2. Structural Parameters Derived from the Model Fits of the Measured XR for C18SH at Different Molecular Coverages<sup>a</sup>**

$A$ $\text{\AA}^2$	$d$ $\text{\AA}$	SU cover. %	$\sigma_1$ $\text{\AA}$	$\sigma_2$ $\text{\AA}$
114	4.8	0	1.2	1.2
48	22.0	40	1.6	1.2
38	22.3	60	1.3	1.3
23	22.2	100	1.6	1.5
20	23.9	100	1.5	2.1
19	25.2	100	2.3	2.6

<sup>a</sup> The table lists the coverage ( $A$ ), the layer thickness ( $d$ ), the percent of the area covered by the standing-up phase in the coexistence range, (SU cover.), and the roughnesses at the thiol/air ( $\sigma_1$ ) and the mercury/thiol ( $\sigma_2$ ) interfaces.

layer includes a contribution from a partial layer of Hg atoms. This model (albeit without the incorporation of the mercury atom into the monolayer) was found to describe well the mercury-supported Langmuir films of alkanes, alcohols, and fatty acids.<sup>38–40</sup> A complete description of the model and the fitting procedures for the XR is given in previous publications.<sup>38–40</sup> The structural parameters obtained from the fits are listed in Table 2. We note that the average area per molecule can be easily calculated from the electron densities, the fractional coverage, and the layer thicknesses refined in the fit. The values thus obtained agree to better than 10% with the nominal average area per molecule ( $A$  in Table 2), calculated from the number of molecules deposited and the trough's area.

The reflectivity curve for  $A = 114$   $\text{\AA}^2/\text{molecule}$  can be reasonably well fitted assuming a single layer (SL) of thiol molecules lying down on the mercury surface. The fit-refined layer thickness, 4.8  $\text{\AA}$ , agrees well with the spacing between adjacent closed-packed chains<sup>53</sup> and also with the molecular width,  $118/25.3 = 4.7$   $\text{\AA}$  obtained from the exclusion area,  $A_1 \approx 118$   $\text{\AA}^2/\text{molecule}$ , of the corresponding isotherm and the extended length of the molecule, 25.3  $\text{\AA}$ . Raising the coverage to 48  $\text{\AA}^2/\text{molecule}$  results in the formation of short-period oscillations in the reflectivity curve, indicating the existence of a thicker layer at the surface. As in previous studies,<sup>39,40</sup> this thick layer consists of a monolayer (ML) of standing-up molecules. The fit yields a layer of thickness  $d = 22.0$   $\text{\AA}$ . Dividing the fit-refined electron

(54) Israelachvili, J. *Intermolecular and Surface Forces*, 2nd ed.; Academic Press: London, 1992.

density of this layer by the 0.30 electrons/Å<sup>3</sup> of a close-packed alkane layer yields a coverage of 40% of the surface area by the standing-up phase, with the remaining 60% of the surface area being covered by the coexisting lying-down phase. With the 25.3 Å length of an extended C18SH molecule, this  $d$  implies that the molecules are tilted by  $\varphi = \arccos(22.3/25.3) \approx 28^\circ$  from the surface normal. These conclusions are strongly supported by the GID data presented below. For  $A = 38 \text{ \AA}^2/\text{molecule}$ , a reflectivity curve very similar to that at  $48 \text{ \AA}^2/\text{molecule}$  is obtained and the fit yields a coverage of 60% of the total area by the standing-up phase, with a slightly higher thickness of 22.3 Å. Increasing the coverage further, we find that the layer thickness does not change. Rather, the area covered by standing-up molecules increases until a full coverage of the surface by the standing-up phase is reached at  $23 \text{ \AA}^2/\text{molecule}$ . Increasing the coverage even further results in a rise in the layer thickness until at  $\sim 19 \text{ \AA}^2/\text{molecule}$  a thickness of 25.2 Å is reached. The equality of the thickness and the extended molecular length implies untilted molecules. Note that the untilted phase was observed only upon cooling below  $T = 10^\circ\text{C}$ . However, this phase remains stable after reheating to room temperature. Without cooling, the maximal thickness that could be obtained was the 23.9 Å listed in Table 2 for  $A = 20 \text{ \AA}^2/\text{molecule}$ . The interfacial roughness stays about the same at 1.2–1.5 Å for most molecular coverages but increases strongly for the two highest coverages reaching  $\sigma \approx 2.6 \text{ \AA}$  for  $A = 19 \text{ \AA}^2/\text{molecule}$ . This may be due to a partial film collapse, which also leads to an increased roughness for the case of *n*-alkane Langmuir films on mercury.<sup>38</sup>

The electron density profiles obtained from the model fits are shown in Figure 4b, where the mercury/thiol interface is at  $z = 0$ , and the Langmuir film resides at negative  $z$  values. These profiles provide a good overview of the phase sequence of the Langmuir film. With increasing coverage, we observe first a lying-down SL phase, the coexistence of the SL phase and the tilted standing-up ML phase, a full-coverage by the tilted ML phase, and finally, after cooling, also an untilted ML phase. The in-plane structure of either the lying-down or the standing-up phases, shown schematically in Figure 1, cannot be determined from reflectivity measurements alone. GID and BR measurements provide important additional information on the structure of these phases. We now proceed to discuss the results obtained from these measurements.

**2. C18SH: Grazing Incidence Diffraction.** A GID pattern measured at a coverage of  $23 \text{ \AA}^2/\text{molecule}$  is shown in Figure 5. For this measurement we summed the GID signal over the full length of the surface-normal-oriented PSD, which covered the  $q_z$  range  $0 < q_z < 0.72 \text{ \AA}^{-1}$ . Due to beam damage, and the large  $q_{||}$  range required, it was not possible to collect data over the whole  $q_{||}$  range of interest in a single scan on the same region of the sample. Thus, the scan was carried out in sections, translating the sample after each section so that the X-rays illuminate a different spot on the sample. The GID pattern is dominated by the broad peak originating from the short range order of the liquid mercury subphase. The peak is centered at  $q_{||} \approx 2.28 \text{ \AA}^{-1}$  and does not depend on the presence or absence of the thiol monolayer. This position is consistent with a short-range liquid order with a mercury layer spacing of 2.76 Å, yielding an atom–atom spacing of 3.18 Å, assuming hexagonal packing. Using the peak's width and the Debye–Scherrer formula,<sup>55</sup> a  $\xi \approx 9 \text{ \AA}$  coherence length is obtained for the short-range liquid order, which corresponds to about three atomic diameters. A comparable  $\xi$  was obtained for the surface of bare mercury.<sup>35</sup> In

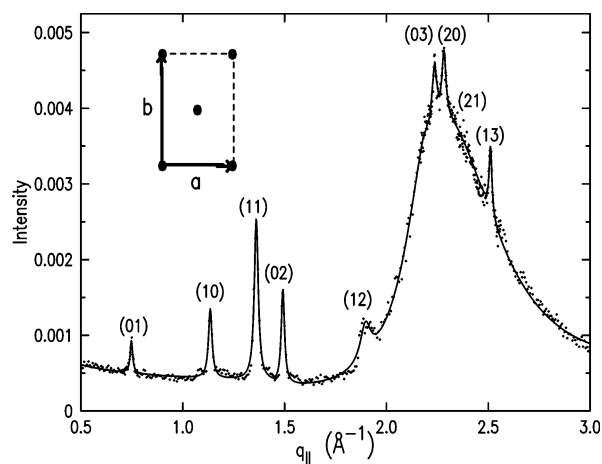


**Figure 5.** Measured (points) GID pattern of C18SH for a molecular coverage of  $23 \text{ \AA}^2/\text{molecule}$  at  $T = 26^\circ\text{C}$ . The smooth line through the points is a guide to the eye. In addition to the broad mercury liquid peak at  $q_{||} \approx 2.28 \text{ \AA}^{-1}$ , eight narrow diffraction peaks, originating in the thiol film can be observed. These can be indexed in a two-dimensional (noncentered) rectangular unit cell shown as an inset.

addition to this broad peak, we observe eight distinct sharp diffraction peaks in the range  $0.5 \text{ \AA}^{-1} \leq q_{||} \leq 3.0 \text{ \AA}^{-1}$ , implying the existence of in-plane long-range order within the thiol film. All peaks can be indexed in a rectangular unit cell with dimensions  $5.52 \times 8.42 \text{ \AA}^2$ , shown in the inset, with two molecules per unit cell, yielding an X-ray-derived area per molecule in the surface plane of  $A_x = 23.2 \text{ \AA}^2/\text{molecule}$ . The GID peak positions, which were measured for several coverages, are summarized in Table 3. In Figure 6 we show the high- $q_{||}$  region of a different GID scan, taken at the same coverage and temperature, which shows a very weak (21) diffraction peak not observed in the scan shown in Figure 5. Except for the weak (21) peak and the (12) peak, which were sometimes not clearly observable above the counting noise in our scans, all peaks shown in Figure 5 were initially observed in all samples measured at  $23 \text{ \AA}^2/\text{molecule}$  but disappeared after extensive beam exposure.

The agreement between the calculated and the measured peak positions is excellent for  $A \geq 22 \text{ \AA}^2/\text{molecule}$ , as can be seen from a comparison of the calculated values in the last row of Table 3 with the measured values. Over the coexistence range,  $73\text{--}23 \text{ \AA}^2/\text{molecule}$ , the variation of the unit cell with  $A$  is practically nil, consistent with the constant  $d$  and consequent tilt angle, obtained from the XR measurements. The only structural variation in this range is in the relative coverage of the surface by the lying down and the standing up phases. The presence of the odd ( $h + k$ ) peaks in the GID spectrum is an unambiguous signature of the unit cell being *noncentered*. SAMs of alkylthiols on a solid Au(111) substrates<sup>17</sup> also show a noncentered unit cell, often referred to by the larger  $c(4 \times 2)$  super-cell. Noncentered cells have not been hitherto reported for monolayers of any chain molecule on Hg<sup>39,40</sup> (except for our previous report on C18SH<sup>45</sup>) or on water,<sup>10</sup> although such cells are obtained on subphases of aqueous solutions of some (though not all) divalent metal ions.<sup>56</sup> To determine the positions of the molecules within the unit cell, the relative intensities of the diffraction peaks are required. Unfortunately, however, the rapid deterioration of the peak intensities due to beam damage excludes here the possibility of such a direct determination. Similar radiation damage effects

(55) Guinier, A. *X-Ray Diffraction*; Freeman: San Francisco, 1963; Chapter 5.

(56) Leveiller, F.; et al. *Science* **1991**, *252*, 1532. Kuzmenko, I.; et al. *Chem. Rev.* **2001**, *101*, 1659. Kmetko, J.; Datta, A.; Evmenko, G.; Dutta, P. *J. Phys. Chem. B* **2001**, *105*, 10818. Kmetko, J.; Datta, A.; Evmenko, G.; Durbin, M. K.; Richter, A. G.; Dutta, P. *Langmuir* **2001**, *17*, 4697.

Table 3. GID Peak Positions for C18SH at Different Molecular Coverages,  $A^a$ 

$A$ $\text{\AA}^2$	$q_z(01)$ $\text{\AA}^{-1}$	$q_z(10)$ $\text{\AA}^{-1}$	$q_z(11)$ $\text{\AA}^{-1}$	$q_z(02)$ $\text{\AA}^{-1}$	$q_z(12)$ $\text{\AA}^{-1}$	$q_z(03)$ $\text{\AA}^{-1}$	$q_z(20)$ $\text{\AA}^{-1}$	$q_z(21)$ $\text{\AA}^{-1}$	$q_z(13)$ $\text{\AA}^{-1}$	<b>a</b> $\text{\AA}$	<b>b</b> $\text{\AA}$
73	0.746	1.140	1.364	1.493						5.51	8.42
48	0.744	1.139	1.361	1.492		2.238	2.280		2.514	5.52	8.42
38			1.363	1.489						5.51	8.43
31		1.139	1.361	1.492						5.52	8.42
25	0.744	1.140	1.365	1.494						5.51	8.42
23	0.747	1.138	1.361	1.494	1.884	2.240	2.280	2.393	2.510	5.52	8.42
22	0.748	1.143	1.367	1.499		2.243	2.284		2.515	5.50	8.40
21	0.750	1.141	1.369	1.511						5.51	8.33
20		1.141	1.368	1.517						5.51	8.29
19(rect)		1.149	1.368	1.512						5.47	8.31
19(hex)			1.498	1.498						4.84	8.39
Calc.	0.746	1.140	1.362	1.492	1.878	2.238	2.280	2.399	2.512	5.51	8.42

<sup>a</sup> The peak positions listed in the last row, marked "calcd", are calculated from a unit cell of  $5.51 \times 8.42 \text{ \AA}^2$ , which fits very well all measured peak positions in the coexistence regime extending from 23 to  $73 \text{ \AA}^2/\text{molecule}$ . The peak positions and the corresponding unit cell dimensions listed in the last two columns vary only slightly over this range. At  $A = 19 \text{ \AA}^2/\text{molecule}$  two unit cells were observed, one hexagonal and the other rectangular. For discussion see text. The experimental uncertainty in the  $q$  values is  $\pm 0.002 \text{ \AA}^{-1}$ .

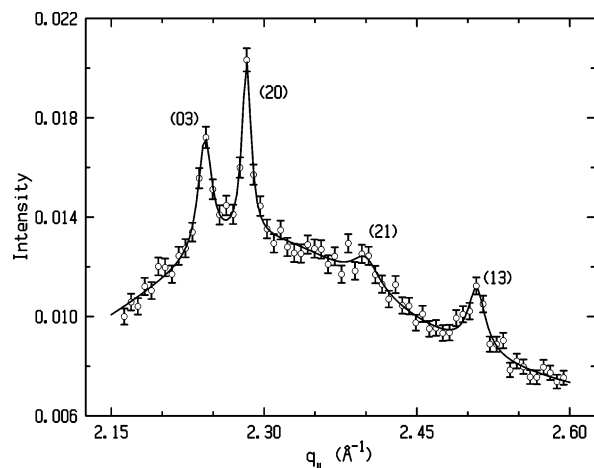


**Figure 6.** Measured GID pattern of C18SH at  $A = 23 \text{ \AA}^2/\text{molecule}$  and  $T = 26 \text{ }^\circ\text{C}$  in the high- $q_{||}$  region. Note the small but distinct (21) peak at  $q_{||} = 2.393 \text{ \AA}^{-1}$ .

have been observed by others<sup>18</sup> for synchrotron radiation studies of alkyl thiol monolayers.

At a coverage of  $19 \text{ \AA}^2/\text{molecule}$  we obtained at room temperature a set of peaks comprising both those of a centered rectangular cell and a hexagonal cell. Lowering the temperature to  $10 \text{ }^\circ\text{C}$  yielded sometimes (though not always) a pure hexagonal phase. The small number of measurements done at low temperatures ( $T \approx 5\text{--}10 \text{ }^\circ\text{C}$ ) does not allow us to determine with confidence which one of the two phases, the hexagonal or the rectangular, is the thermodynamically stable one and which is the kinetically stabilized one. This point is further discussed below. However, the present hexagonal phase is the same as the LS phase observed in Langmuir films of many amphiphiles on water at high coverages.<sup>10</sup> The details of the molecular tilt and of the transition between the tilted and untilted standing-up phases are discussed in the next section.

**3. C18SH: Bragg Rods and Molecular Tilts.** Figure 7 shows an equal-intensity contour plot, in the  $(q_{||}, q_z)$  plane, of the GID peaks at  $q_{||} = 1.14, 1.36, \text{ and } 1.49 \text{ \AA}^{-1}$ . This plot displays the distribution of the intensity along the  $q_z$  axis at the  $q_{||}$  positions of the peaks, i.e., the Bragg rods, which provide information on the molecular tilts and surface-normal dimensions of the diffracting objects. The position of the off-axis peak provides an accurate measure of the molecular tilt. The profile widths of the Bragg rods are very different from each other, and should have, therefore, different origins. The (02) rod has the conventional shape of a typical rod of a Langmuir film comprising standing-

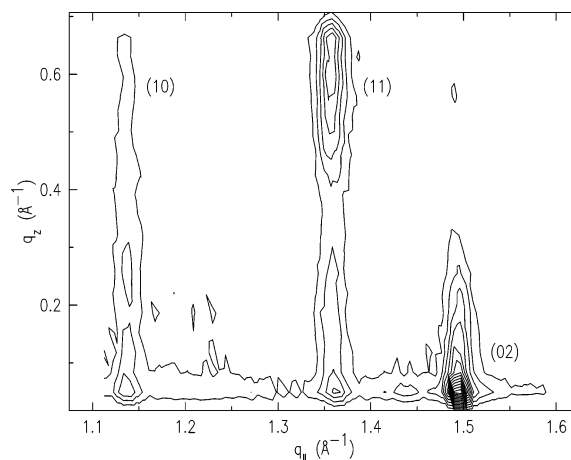


**Figure 7.** Equal-intensity contour plot of a portion of the GID pattern shown in Figure 5. Note, in particular, the low-intensity but extended (10) peak at  $q_{||} = 1.14 \text{ \AA}^{-1}$ , resulting from the noncentered unit cell of the thiol headgroups. (10) and (02) are typical of the broad and the sharp BRs, respectively, discussed in the text.

up molecules. Its half-intensity decay length in the  $q_z$  direction,  $\Delta q_z \approx 0.15 \text{ \AA}^{-1}$ , is consistent with the extended molecular length. By contrast, the (10) rod, while similar to the (02) rod in having its intensity maximum at  $q_z \approx 0 \text{ \AA}^{-1}$ , is much more extended in the  $q_z$  direction, exceeding the  $q_z$  range measured here,  $0 \leq q_z \leq 0.72 \text{ \AA}^{-1}$ . It must, therefore, originate in a layer much thinner than the molecular length, of order of several  $\text{\AA}$ . The (11) rod clearly contains two peaks: a broad one centered at  $q_z \approx 0 \text{ \AA}^{-1}$  and a sharp one centered at  $q_z = 0.6 \text{ \AA}^{-1}$ . It seems, therefore, to be a sum of two rods, one similar to the (10) rod and the other similar to the (02) rod.

A clearer view of the measured BRs of the four lowest-order peaks is shown in Figure 8 (open circles), after background subtraction. The measured BRs were fitted by the analytical expression derived in a previous publication,<sup>57</sup> which assumes a rotator phase packing, in which each molecule occupies a cylindrical volume centered on the molecule's long axis. The fits are shown in Figure 8 (lines) and exhibit excellent agreement with the measured points. The BR of the (01) peak, which extends to  $q_z \geq 0.72 \text{ \AA}^{-1}$ , yields a layer of thickness  $d \leq 4 \text{ \AA}$ , the most likely candidate for which is the layer of thiol headgroups bound to the mercury surface. The broad (10) rod yields a layer thickness

(57) Lekner, J. *Theory of Reflection*; Martinus Nijhoff: Dordrecht, 1987. Abeles, F. *Ann. Phys. (Paris)* **1950**, *5*, 596. Ocko, B. M.; Wu, X. Z.; Sirota, E. B.; Sinha, S. K.; Gang, O.; Deutsch, M. *Phys. Rev. E* **1997**, *55*, 3164.

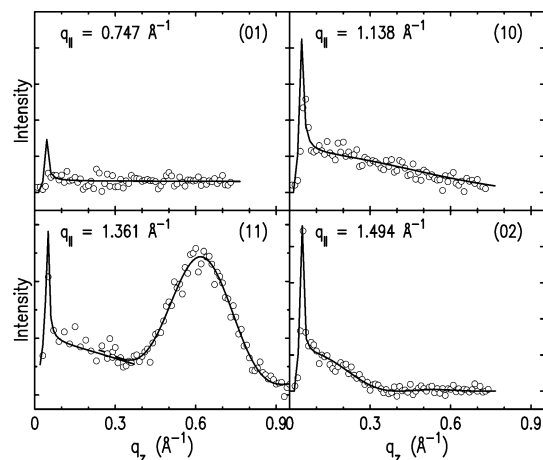


**Figure 8.** Measured (open circles) and model-fitted (lines) BRs for the four lowest  $q_{||}$  GID peaks in Figure 5.

of  $d = (6 \pm 2) \text{ \AA}$ . Therefore, this rod may originate from the head group/mercury complex plus one or two carbons of the hydrocarbon chain of a standing-up molecule. The thickness of this layer would also agree very well with that of a single layer of lying-down molecules, implying a partial coverage of the surface by the lying-down single-layer phase even at these high coverages, well outside the coexistence plateau of the isotherm. However, it seems unlikely that the peak positions of the lying-down phase would coincide exactly with those of the standing-up phase. Also, the layer spacing of  $5.51 \text{ \AA}$  is too large for a parallel ordering of lying-down molecules. The broad component of the (11) rod could possibly originate either in a lying-down phase or in the headgroups of the standing-up phase. The former explanation seems unlikely as we do not observe, for any coverage, diffraction peaks of a pure lying-down phase. Moreover, the intensity ratio of the broad and the sharp components of the (11) peak changes very little over the whole coverage range and seems inconsistent with coexistence.

A careful examination of all BRs reveals that the odd ( $h + k$ ) peaks comprise only broad BRs. The sharp BR components are found only in the even ( $h + k$ ) peaks (although the even ( $h + k$ ) may also include broad BR contributions). Thus, the odd ( $h + k$ ) GID peaks originate exclusively in the headgroups' layer, while the tails' and headgroups' layers contributes to even ( $h + k$ ) GID peaks. This leads to the conclusion that while the headgroups order in a *noncentered* rectangular cell, the tails order in a *centered* rectangular cell.<sup>58</sup>

We discuss first the centered unit cell, based on the sharp components of the even ( $h + k$ ) BRs. The sharp components of the (11) and (02) rods are the same as the commonly observed rods of Langmuir monolayers on water for a centered rectangular unit cell with tilted molecules.<sup>10</sup> Their fit, shown in Figure 8, results in a tilt angle of  $\varphi = 27^\circ$ , close to the tilt angle extracted from the XR above, and an azimuthal rotation of  $\chi \leq 4^\circ$  from the nearest-neighbor (NN) tilt direction. This is the tilt required for a 2-carbon shift between adjacent chains, which moves the tooth of one zigzag chain to the next depression in the adjacent zigzag chain. With the surface-parallel unit cell dimensions derived above, this tilt yields a unit cell of dimensions  $5.51 \text{ \AA} \times \cos 27.0^\circ \times 8.42 \text{ \AA} = 4.91 \times 8.42 \text{ \AA}^2$  in the plane perpendicular to the molecular long axis. The resultant X-ray-derived area per molecules in that plane,  $A_{\perp} = 20.7 \text{ \AA}^2/\text{tail}$ , is typical of a rotator phase, rather than a herringbone-ordered crystalline phase for

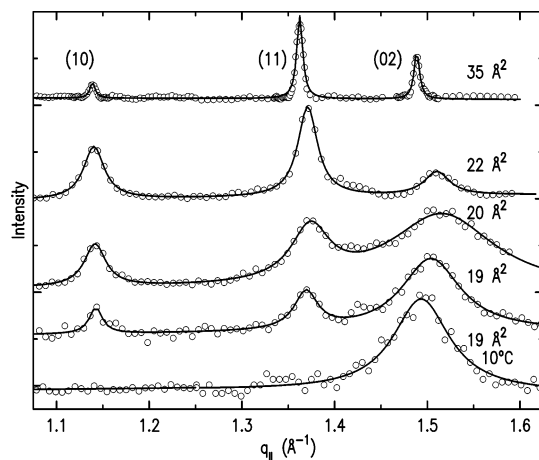


**Figure 9.** GID pattern of C18SH at the transition from the standing-up tilted phase to the untilted phase. The variations in the pattern, and in the intensities and widths of the peaks, with  $A$  (listed for each curve) are discussed in the text.

which  $18.5 \text{ \AA}^2/\text{molecule} \lesssim A_{\perp} \lesssim 19.0 \text{ \AA}^2/\text{molecule}$ .<sup>10,59</sup> This supports the use of the rotator model in the BR fits discussed above. Moreover, the ratio  $8.42/4.91 \approx \sqrt{3}$ , proves that the tails pack hexagonally in this plane. These results identify the structure of the tails' layer as the  $L_{2d}$  phase of fatty acid monolayers on water.<sup>10</sup>

The noncentered order of the headgroups can be traced to the chemistry of the thiol moiety. As the sharp and broad BRs originate, respectively, in the tails and headgroups of the alkylthiols, the ratio of their contributions (integrated over  $q_z$ ) to the intensity of the low- $q_{||}$  GID peaks in Figure 5 is related to the ratio  $R_e$  of the number of scattering electrons in these two parts of the molecule. The 1:1.5-to-1:3 BR intensity ratio found implies an  $R_e$  significantly larger than the 17:145 expected from the  $\text{SH}/\text{CH}_3(\text{CH}_2)_{17}$  composition of the molecule. This argues against the two-molecule S–S hybridization (disulfide), suggested for alkylthiols on Au,<sup>17</sup> as the origin of the noncentered headgroups' cell, since this does not significantly change  $R_e$ . Rather, the high-intensity ratio suggests the incorporation of a single Hg atom per two thiol molecules into the headgroups' layer, forming a covalent S–Hg–S bond. This conclusion is supported by the 1:2 Hg/thiol stoichiometry found in bulk Hg-thiolates,<sup>23</sup> where the strong covalent S–Hg–S bond is found to involve a transfer of one electron per thiol with the corresponding loss of the terminal hydrogen. In contrast, on Au(111), only a partial transfer,  $\sim 0.3$  electrons/thiol, is found.<sup>60</sup> We also note that the equal  $q_{||}$  widths of the odd- and even-order GID peaks in Figure 5 imply not only equal crystalline coherence lengths for both the tails' and headgroups' layers, but also a long-range orientational order for the S–Hg–S bonds.

We now discuss the first-order transition from the  $27^\circ$  tilted  $L_{2d}$  phase to the untilted, LS standing-up phase at  $A \approx 20\text{--}23 \text{ \AA}^2/\text{molecule}$ . Figure 9 shows measured (open circles) and Lorentzians-fitted (lines) GID patterns for coverages in the transition region. As discussed above, no significant variation in peak positions of the tilted phase, shown in the uppermost curve, are observed for  $A$  above  $\sim 23 \text{ \AA}^2/\text{molecule}$ . As  $A$  decreases below  $23 \text{ \AA}^2/\text{molecule}$ , a small upward shift in the  $q_{||}$  positions of the diffraction peaks are observed. A further decrease in  $A$  to  $20 \text{ \AA}^2/\text{molecule}$  and then to  $19 \text{ \AA}^2/\text{molecule}$  results in a considerable decrease in the intensities of the (10) and the (11)

(58) The structure could also be described by an oblique lattice of tails, with a  $1 \times 2$  superlattice of headgroups.

(59) Small, M. *The Physical Chemistry of Lipids*; Plenum: New York, 1986; p 11.

(60) Krysinski, P.; Chamberlain, R. V.; Majda, M. *Langmuir* **1994**, *10*, 4286.

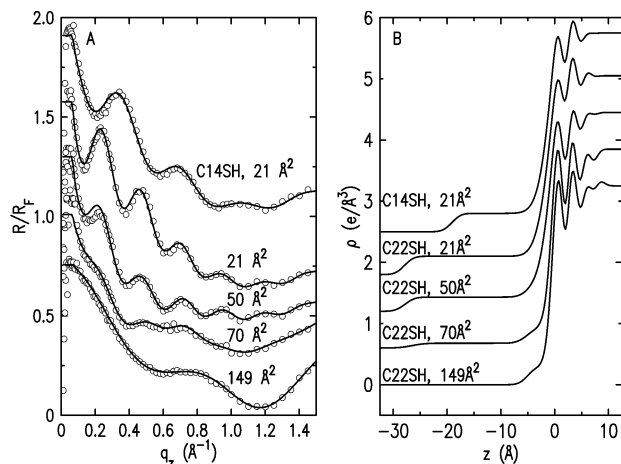


**Figure 10.** (a) Measured XR (points) and model fits (line) for the indicated coverages of C22SH and for a high-coverage phase of C14SH. (b) The corresponding surface-normal density profiles derived from the fits.

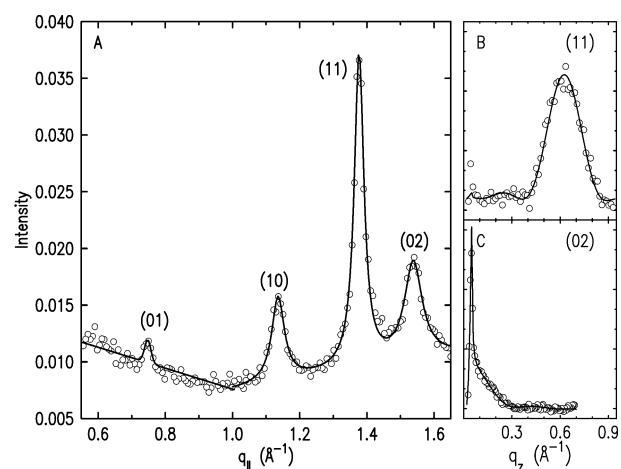


**Figure 11.** (a) Measured (open circles) GID and (b,c) BR scans, with model fits (lines), for the pure standing-up monolayer phase of C22SH at a coverage of 21  $\text{\AA}^2/\text{molecule}$  and  $T = 26$  °C. The BR fits yield a tilt angle of  $\varphi = 27.6^\circ$  from the surface normal in the nearest-neighbor direction.

peaks and a commensurate increase in the intensity of the (02) peak. Since the relative intensities of the odd-order peaks to the (11) peak remains constant, the S–Hg–S bond order in the tilted phase appears to remain unaffected by changes in  $A$ . This suggests that the transition is first-order. The limit of this sequence leads to a possible transition from a tilted rectangular phase to a hexagonal phase, having lattice parameters (in rectangular coordinates)  $a = 4.84$   $\text{\AA}$  and  $b = 4.84 \times \sqrt{3} = 8.38$   $\text{\AA}$ , which yield a molecular area of 20.3  $\text{\AA}^2/\text{molecule}$ . These values agree well with those observed (admittedly not always, as discussed above) for the pure hexagonal low-temperature ( $T = 10$  °C) phase. These values are typical for the hexagonal LS phase of Langmuir films of chain molecules on aqueous subphases.<sup>10</sup>

The peak position and intensity changes across the transition region are accompanied by changes in the peak widths. The width of the rectangular unit cell peaks (10) and (11) are observed to broaden considerably from the resolution-limited value of  $\Delta q_{||} \approx 0.007$   $\text{\AA}^{-1}$  at 35  $\text{\AA}^2/\text{molecule}$  to  $\Delta q_{||} \approx 0.04$   $\text{\AA}^{-1}$  at 20  $\text{\AA}^2/\text{molecule}$ . The (02) peak, located very close to the single peak of the hexagonal phase, broadens even more, to  $\Delta q_{||} \approx 0.09$   $\text{\AA}^{-1}$  at 20  $\text{\AA}^2/\text{molecule}$ , then reduces to  $\Delta q_{||} \approx 0.07$   $\text{\AA}^{-1}$  at 19  $\text{\AA}^2/\text{molecule}$  at  $T = 10$  °C. The resolution-limited peak width of the rectangular phase indicates that the coherence length of the

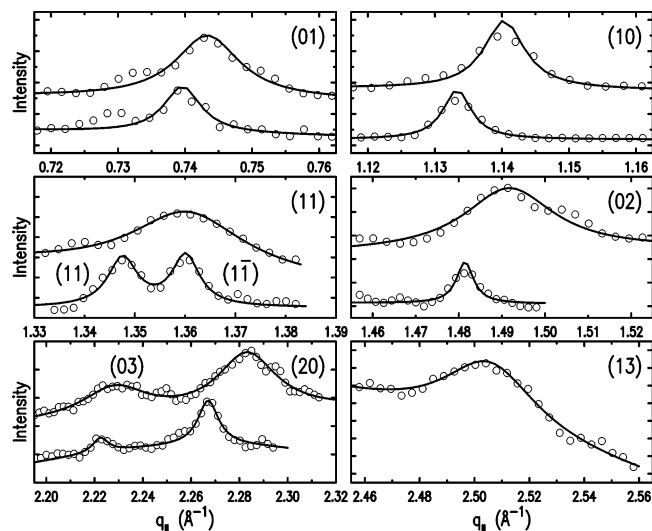


**Figure 12.** Measured (open circles) and Lorentzian-fitted (lines) GID scans for C14SH for coverages of 83 (lower curves) and 19  $\text{\AA}^2/\text{molecule}$  (upper curves) at  $T = 26$  °C. Note the splitting of the (11) peak at low coverage, indicating a slight deviation of the unit cell from rectangularity.

**Table 4. Peak Positions Derived from the Measured GID Patterns for C22SH at Different Coverages<sup>a</sup>**

$A$ $\text{\AA}^2$	$q(01)$ $\text{\AA}^{-1}$	$q(10)$ $\text{\AA}^{-1}$	$q(11)$ $\text{\AA}^{-1}$	$q(02)$ $\text{\AA}^{-1}$	$a$ $\text{\AA}$	$b$ $\text{\AA}$
70	0.748	1.143	1.370	1.506	5.50	8.36
23		1.137	1.366	1.516	5.53	8.29
21		1.134	1.370	1.539	5.54	8.17

<sup>a</sup> The corresponding rectangular unit cell dimensions are listed in the last two columns. As in Table 3, the experimental uncertainty of the  $q$  values is  $\pm 0.002$   $\text{\AA}^{-1}$  but increases to  $\pm 0.01$   $\text{\AA}^{-1}$  for the  $q(02)$  at the highest coverage.

crystalline order of that phase is  $\xi \geq 1000$   $\text{\AA}$ . The hexagonal phase is, however, rotator-like, with a coherence length of only  $\xi \approx 90$   $\text{\AA}$ . The fact that for  $A = 20$   $\text{\AA}^2$  the (02) peak is considerably broader than the (10) or the (11) peaks implies a phase coexistence between the tilted rectangular phase and the hexatic-like hexagonal phase. The reduction in  $\xi$  upon the transition to the hexagonal phase reflects a packing frustration, which may originate in a S–Hg–S bond orientation disorder. This may arise, in turn, from the absence of a unique preferred direction for the bond in the hexagonal phase. The reduction in the range of the orientational order of the S–Hg–S bonds may provide an explanation for the absence of the odd-order peaks in this phase. A similar explanation accounted for the reduction in coherence length upon lateral polymerization in monolayers of octadecyltrichloromethylsilane (OTS) on silicon.<sup>15</sup> The broadening is possibly enhanced in the coexistence regime by the strains at the interfaces between grains of different symmetries and slightly different lattice constants.

Finally, we note that the rectangular  $L_{2d}$  and the hexagonal LS phases found here are very similarly packed in the plane perpendicular to the molecular long axis  $A_{\perp}$ . In the tilted phase  $A_{\perp} = 20.7$   $\text{\AA}^2/\text{tail}$  whereas in the hexagonal phase  $A_{\perp} = 20.3$   $\text{\AA}^2/\text{molecule}$ . Thus, the chain packing density in the hexagonal LS phase is only slightly higher than that in the tilted  $L_{2d}$  phase.

**4. C22SH.** The similarity of the isotherms of C14SH and C22SH in Figure 3 to that of C18SH implies similar phases and a similar phase sequence with decreasing  $A$ . This expectation is indeed supported by the XR and GID measurements, discussed below. Figure 10a presents measured (open circles) and model-fitted (lines) XR for C22SH and C14SH (topmost curve), and the

**Table 5. Peak Positions Derived from the Measured GID Patterns for C14SH at Different Molecular Coverages<sup>a</sup>**

$A$ $\text{\AA}^2$	$q(01)$ $\text{\AA}^{-1}$	$q(10)$ $\text{\AA}^{-1}$	$q(11)$ $\text{\AA}^{-1}$	$q(1\bar{1})$ $\text{\AA}^{-1}$	$q(02)$ $\text{\AA}^{-1}$	$q(03)$ $\text{\AA}^{-1}$	$q(20)$ $\text{\AA}^{-1}$	$q(13)$ $\text{\AA}^{-1}$	$\mathbf{a}$ $\text{\AA}$	$\mathbf{b}$ $\text{\AA}$	$\gamma$ $^\circ$
83	0.740	1.133	1.347	1.361	1.481	2.222	2.267		5.54	8.49	89.4
40	0.740	1.135	1.348	1.362	1.480				5.54	8.49	89.4
24	0.743	1.138	1.352	1.363	1.486	2.225	2.277		5.52	8.46	89.5
19	0.744	1.140	1.360	1.360	1.491	2.229	2.283	2.506	5.51	8.44	90.0

<sup>a</sup>  $\gamma$  is the angle between the lattice vectors  $\mathbf{a}$  and  $\mathbf{b}$ .

surface-normal density profiles derived from the fits (Figure 10b). At low coverage,  $A = 149 \text{ \AA}^2/\text{molecule}$ , the XR measurements of C22SH show a single layer of lying-down molecules,  $5.0 \text{ \AA}$  thick. On increasing the coverage ( $70$  and  $50 \text{ \AA}^2/\text{molecule}$ ) we first observe a coexistence between the lying-down phase and a standing-up tilted phase and finally ( $21 \text{ \AA}^2/\text{molecule}$ ) a pure standing-up monolayer phase of tilted molecules. The fits for coverages of  $70$  and  $50 \text{ \AA}^2/\text{molecule}$  show coverages of  $30\%$  and  $80\%$ , respectively, of the surface area by the standing-up monolayer, with a thickness of  $26.5$  and  $27.8 \text{ \AA}$ , respectively. The pure standing-up monolayer phase at a coverage of  $21 \text{ \AA}^2/\text{molecule}$  is  $27.9 \text{ \AA}$  thick, the same as that at  $A = 50 \text{ \AA}^2/\text{molecule}$ . Compared to the  $30.5 \text{ \AA}$  length of an extended C22SH molecule, these thicknesses yield tilt angles of  $\varphi \approx \arccos(26.6/30.5) \approx 29^\circ$  for  $70 \text{ \AA}^2/\text{molecule}$  and  $\varphi \approx \arccos(27.9/30.5) \approx 24^\circ$  for  $50 \text{ \AA}^2/\text{molecule}$ .

Figure 11 shows the measured and Lorentzian-fitted GID pattern of C22SH, along with the BRs of the (11) and the (02) diffraction peaks. The peak positions for all GID scans are summarized in Table 4. In the vicinity of the (01) peak the GID was measured only for  $A = 70 \text{ \AA}^2/\text{molecule}$ , and the corresponding (01) peak positions are therefore absent from the table for  $A = 23$  and  $21 \text{ \AA}^2/\text{molecule}$ . The other three diffraction peaks were measured for all coverages. As in the more detailed study of C18SH discussed above, for the highest coverage, the diffraction peaks are consistent with a rectangular unit cell of dimensions  $\mathbf{a} = 5.54 \text{ \AA}$  and  $\mathbf{b} = 8.17 \text{ \AA}$ . The fits to the BR yield a tilt angle of  $\varphi = 27.5^\circ$ , independent of coverage. Similar to C18SH, the tilt is in the nearest-neighbor direction. The tilt angle and its direction lead to a unit cell in the plane perpendicular to the molecular long axis which shrinks slightly with increasing coverage  $A$ , from  $4.87 \times 8.36 \text{ \AA}^2$  at  $A = 70 \text{ \AA}^2/\text{molecule}$  to  $4.91 \times 8.17 \text{ \AA}^2$  at  $A = 21 \text{ \AA}^2/\text{molecule}$ . This corresponds to  $A_\perp = 20.4$  and  $20.0 \text{ \AA}^2/\text{molecule}$ , respectively, slightly higher than that of C18SH in the corresponding tilted phase. The finite-intensity (01) and (10) diffraction peaks and their Bragg rods show that the thiol headgroups are ordered in a noncentered rectangular unit cell.

These observations are very similar to those found for C18SH; upon increasing the coverage, the long lattice parameter  $\mathbf{b}$  shrinks and the unit cell in the plane perpendicular to the molecular long axis increasingly diverges from hexagonal symmetry. The ratio  $\mathbf{b}/\mathbf{a}$  changes from  $1.72$  for a coverage of  $70 \text{ \AA}^2/\text{molecule}$  to  $1.66$  for a coverage of  $21 \text{ \AA}^2/\text{molecule}$  as compared to the ratio of  $\mathbf{b}/\mathbf{a} = 1.73$  for a hexagonal unit cell. Unlike C18SH, a hexagonal untilted phase was not observed, perhaps because no temperature-dependent measurements have been carried out.

5. *C14SH*. Similar to C18SH and C22SH, the XR measurements on C14SH also show the formation of a single layer of lying-down molecules, followed, upon increasing the coverage, by a coexistence region between standing-up and lying-down phases and, finally, by a single-phase layer of tilted standing-up molecules. The XR of the latter phase is shown as the topmost curve in Figure 10. The fitted layer thickness is  $d = 19.1 \text{ \AA}$ , indicating a molecular tilt of  $\varphi = \arccos(19.1/20.2) \approx 19^\circ$ , somewhat smaller than those of C18SH and C22SH. The GID

peaks measured (open circles) and fitted (lines) for coverages of  $83$  and  $19 \text{ \AA}^2/\text{molecule}$  are shown in Figure 12, and their peak positions are summarized in Table 5.

The same diffraction peaks as those of C18SH are observed, except that for C14SH we did not observe the odd ( $h + k$ ) higher-order peaks (12) and (21), which even for C18SH were rather weak and sometimes absent. Thus, the unit cell of all thiol monolayers studied here are similar. In contrast with C18SH, however, for C14SH at all coverages (except for the highest one) the (11) diffraction peak is split into two peaks. This can be accounted for by assuming a small deviation from a rectangular unit cell, which can be quantified by allowing the angle  $\gamma$  between  $\mathbf{a}$  and  $\mathbf{b}$  to deviate from  $90^\circ$ . We obtain here  $\gamma \approx 89.4^\circ$  for all but the highest coverage. This distortion causes the (11) and ( $1\bar{1}$ ) diffraction peaks not to overlap. For the highest coverage we obtain  $\gamma = 90^\circ$  and the (11) and ( $1\bar{1}$ ) diffraction peaks merge into a single peak. Similar to C18SH, upon decreasing  $A$ ,  $\xi$  decreases from a resolution limited value of  $\xi > 1000 \text{ \AA}$  at  $83 \text{ \AA}^2/\text{molecule}$  to  $\sim \xi = 200 \text{ \AA}$  at  $19 \text{ \AA}^2/\text{molecule}$ . The unit cell also shrinks slightly, as observed clearly in Figure 12 from the upshift of the  $q_{11}$  positions of the GID peaks at  $19 \text{ \AA}^2/\text{molecule}$  from those at  $83 \text{ \AA}^2/\text{molecule}$ .

The BR of the four lowest-order diffraction peaks are shown in Figure 13. The BR for (01) and (10) are very extended, indicating that they originate in a very thin ordered layer of thickness  $\sim 5 \text{ \AA}$ , consistent with the C14SH XR fits and the results for C18SH. The BR of the (11) peak has two components: a broad one centered at  $q_z \approx 0 \text{ \AA}^{-1}$  and a sharp one peaked at  $q_z \approx 0.5 \text{ \AA}^{-1}$ . The rod shape and  $q_z$  and  $q_{11}$  peak positions of the sharp component of the (11) and the (02) peaks are consistent with a nearest-neighbor tilt direction and a tilt angle of  $\varphi = 22.1^\circ$ . Increasing the coverage from  $83$  to  $19 \text{ \AA}^2/\text{molecule}$  results in a reduction of the corresponding tilt angle from  $24.4^\circ$  to  $22.1^\circ$ . Using the tilt angles for the different coverages, we can calculate the unit cell in the plane perpendicular to the long axis of the molecules. This results in a unit cell of  $5.05 \times 8.49 \text{ \AA}^2/\text{molecule}$  for the lowest coverage and  $5.11 \times 8.44 \text{ \AA}^2/\text{molecule}$  for the highest coverage. Both are close to a hexagonal unit cell with fairly large molecular areas of  $21.4$  and  $21.6 \text{ \AA}^2/\text{molecule}$ , respectively. Finally, we note that these unit cell dimensions are slightly larger than those of C18SH and C22SH.

**C. The Phase Diagram.** The X-ray data presented above for C14SH, C18SH, and C22SH monolayers on the surface of liquid mercury provide insight into the chain-length-dependent phase diagram. We first summarize the structural features found in the X-ray measurements for these molecules.

For low coverage, all the alkyl thiols studied exhibit a SL of lying-down molecules. No GID peaks were found in this phase for any molecular length studied here, indicating that the lying-down phase is disordered.

The standing-up phases of all the alkyl thiols have a rectangular unit cell, containing two molecules. In the coexistence range of the standing-up and the lying-down phases the molecules of the standing-up phase are always tilted toward the nearest-neighbor direction. The short axis of the unit cell is  $\mathbf{a} \approx 5.51 \text{ \AA}$ . The long axis of the unit cell,  $\mathbf{b}$ , decreases with increasing chain length.

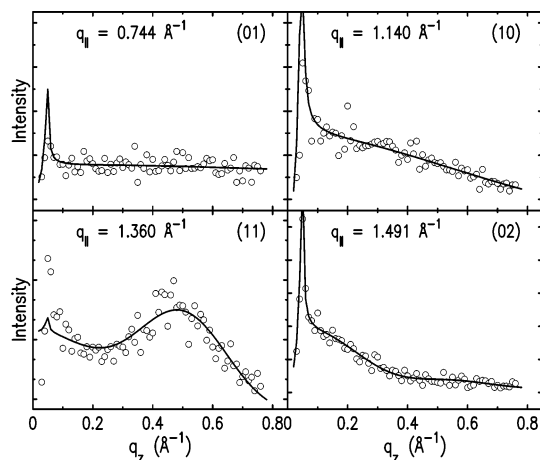


**Figure 13.** BRs of the four lowest-order GID peaks of the standing-up phase of C14SH at  $19 \text{ \AA}^2/\text{molecule}$  and  $T = 26 \text{ }^\circ\text{C}$ .

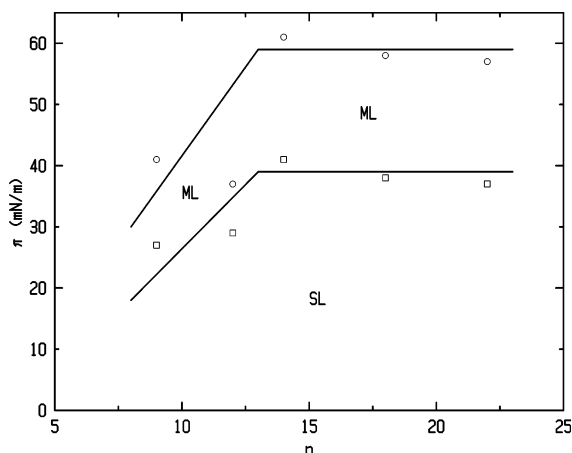


**Figure 14.** Pressure ( $\pi$ )–chain length ( $n$ ) phase diagram for Langmuir films of alkyl-thiols on mercury. SL denotes a single layer of lying-down molecules. ML denotes a monolayer of standing-up molecules. Open circles denote the collapse pressure of the ML phase, and open squares denote the transition from the lying-down phase to the standing-up phase. Lines are guides to the eye.

It is, respectively, 8.44, 8.42, and  $8.17 \text{ \AA}$  for C14SH, C18SH, and C22SH. The tilt angles increase with molecular chain length from  $22^\circ$  to  $24^\circ$  for C14SH to  $27^\circ$  for C18SH to  $28^\circ$  for C22SH. All of these values are not too far from the  $27^\circ$  tilt, required to move one carbon of a given chain from one hollow in an adjacent zigzag to the next one. These values also indicate that in the plane perpendicular to the long axis of the molecule the chains are ordered very close to a hexagonal packing, similar to the  $L_{2d}$  phase of Langmuir films of water.<sup>10</sup>

The molecular area of the rectangular unit cell in the plane perpendicular to the long axis of the molecules decreases with increasing chain length from  $A_\perp = 21.6 \text{ \AA}^2/\text{molecule}$  for C14SH to  $A_\perp = 20.7 \text{ \AA}^2/\text{molecule}$  for C18SH and to  $A_\perp = 20.0 \text{ \AA}^2/\text{molecule}$  for C22SH. For all investigated alkyl-thiols, the hydrocarbon chains form a centered rectangular unit cell while the thiol headgroups form a noncentered unit cell, which gives rise to odd ( $h + k$ ) GID peaks. The mercury atoms appear to be chemically bound to the thiol headgroup forming a thiolate salt with a 2:1 stoichiometry. The S–Hg–S bonds exhibit long-range orientational order. This conclusion is supported by the intense higher-order diffraction peaks and the resolution-limited width of the diffraction peaks for the tilted monolayer phase. A schematic view of the real space behavior with increasing coverage is shown in Figure 1.

The ( $n, \pi$ ) phase diagram emerging from our measurements is shown in Figure 14. For the longer chain alkyl-thiols,  $n \geq 14$ , the single lying-down layer exerts a pressure of up to  $40 \text{ mN/m}$  and above that transforms to a monolayer of standing-up molecules. For smaller chain lengths, the transition pressure is reduced, similar to the findings for alcohols and fatty acids on mercury.<sup>37,38,40</sup> However, in contrast with those molecules, which form multiple-layer phases of lying-down molecules (in some cases up to four layers), for thiols only a single layer of lying-down molecules is observed regardless of chain length. This can be attributed to the much higher affinity of the thiol headgroup to mercury as compared to an alcohol or a fatty acid headgroup. To maximize the sulfur–mercury contact this high affinity induces a standing-up molecular orientation at a much lower pressure than those observed in alcohols ( $\sim 50 \text{ mN/m}$  for  $n \geq 16$ ) and fatty acids ( $\sim 46 \text{ mN/m}$  for  $n \geq 14$ ). This strong affinity induces also a much larger pressure range of existence for the standing-up phase,  $40 \leq \pi \leq 60 \text{ mN/m}$ , vs  $50 \leq \pi \leq 54$  for alcohols and  $46 \leq \pi \leq 51$  for fatty acids. Unfortunately, since very little thermodynamic data is available in the literature on the heat of vaporization of alkyl thiols, these considerations cannot be reliably quantified to yield the adsorption energies of alkyl-thiols on mercury, as done for alcohols and fatty acids.<sup>37,38,40</sup>

Finally, we note that the phase diagram in Figure 14 may comprise other phases, over limited ( $n, \pi$ ) ranges. One such phase is an untilted hexagonal LS phase which may exist over a narrow  $\pi$ -range just below  $\pi_c$ , as indicated by the C18SH results discussed above. Another example is the slightly nonrectangular tilted ML phase found for C14SH, which may exist also for lower chain lengths. An exact determination of the  $n$  and  $\pi$  ranges of existence of these phases would require further studies.

## V. Conclusion

The big differences among Langmuir films of different chain molecules on mercury in the adsorption behavior, the phases observed, and their sequence, as found in our previous studies of alkanes,<sup>38</sup> alcohols,<sup>39</sup> and fatty acids<sup>38–40</sup> and in the present study of thiols, can be traced mainly to the different headgroup–subphase interactions. While the hydrocarbon chains physisorb on the mercury surface with a heat of adsorption of roughly  $\Delta H_{\text{ads}} \approx 5 \text{ kJ/mol}$  per  $\text{CH}_2$  group<sup>38</sup> for all molecules, the adsorption energy of the headgroups varies considerably from the methyl headgroup of normal alkanes ( $5.4 \text{ kJ/mol}$ <sup>38</sup>), to the hydroxyl group of alcohols ( $21 \text{ kJ/mol}$ <sup>39</sup>), to the carboxyl of fatty acids ( $28 \text{ kJ/mol}$ <sup>39</sup>), to thiols ( $128 \text{ kJ/mol}$ <sup>14</sup> on Au, and similar or larger for Hg<sup>35</sup>). For the methyl-terminated alkanes, the difference in adsorption energy between a  $\text{CH}_2$  chain and the  $\text{CH}_3$  headgroup is too small to cause the molecules to stand up, regardless of the surface pressure. The magnitude of the adsorption energy of the alcohol and the fatty acid headgroup are comparable to each other and are 4–5 times larger than that of a  $\text{CH}_2$  group. Consequently, both molecules form lying-down single- and double-layer films at low coverages and surface pressures, but as the coverage increases, so does the surface pressure, and under the combined inducement of the surface pressure and the headgroup's high adsorption energy onto the mercury, the molecules stand up to maximize the headgroup–mercury contact. As the hydroxyl headgroup's adsorption energy is slightly smaller than that of the carboxylic headgroup, alcohols can form up to four lying-down layers before the pressure rises high enough to induce a standing-up layer, while the fatty acids form only two lying-down layers before the formation of the standing-up phase occurs.

The structure of the standing up phases of both the alcohol and the fatty acid molecules are dominated by their chain–chain

**Table 6. Summary of the X-ray-Derived Molecular Areas, the Lattice Constants, and Tilts for C14SH, C18SH, and C22SH in their High-Coverage Tilted Rectangular Phases<sup>a</sup>**

<i>n</i>	$A_{\parallel}$ Å <sup>2</sup> /mol.	$A_{\perp}$ Å <sup>2</sup> /mol.	$A_{\perp}$ Å <sup>2</sup> /mol.	$\varphi$ °	$a_{\parallel}$ Å	$a_{\perp}$ Å	$b = b_{\perp}$ Å	$b_{\perp}/\sqrt{3}a_{\perp}$
14	19	23.3	21.6	22.1	5.51	5.11	8.44	0.95
18	23–73	23.2	20.7	27.0	5.51	4.91	8.42	0.99
22	21	22.5	20.0	27.5	5.51	4.88	8.17	0.97
18(hex)	19	20.3	20.3	0.0	4.84	4.84	8.39	1.00

<sup>a</sup> The values for the hexagonal untilted phase of C18SH are listed in the last row.

interaction and therefore show the same phases, both almost identical to those of their respective Langmuir films on water. The only difference is that the tilted phases seem to be generally suppressed for these molecules on a mercury subphase as compared to an aqueous subphase. For the thiol headgroup, we have the strongest adsorption onto the mercury surface. Consequently, the thiols form only a single layer of lying-down molecules before the standing-up layer is formed.

The strong affinity of the thiol headgroup toward the mercury results in an additional important structural motif. While the alkyl chains form a centered rectangular unit cell, which is close to hexagonal in the plane perpendicular to the molecular long axis, the thiol headgroups deviate from this simple symmetry and form a noncentered unit cell. This is due to the formation of S–Hg–S bonds (mercury thiolate salt) which prefer a somewhat smaller molecular spacing than that of the chains. The postulated formation of the salt could also alter the order the topmost mercury layer, which, in turn, causes the higher-order diffraction peaks to be intense enough to be observed. It should be noted that the mercury atoms which form the S–Hg–S bonds are not metallic since their valence electrons are not contributed to the electron sea of the liquid metal. With a 3.18 Å average atom–atom spacing at the mercury surface, the ~46 Å<sup>2</sup> area of the unit cell covers more than five surface atoms of mercury. Of these, one mercury atom is bound to two terminal sulfur atoms of the thiols and the remaining, more than four mercury atoms on average, are metallic.

The chain length dependent molecular areas and unit cell dimensions for the LMs studied here are summarized in Table 6. As the last column shows, the distortion from a hexagonal packing ( $b_{\perp}/(\sqrt{3}a_{\perp}) = 1$ ) are less than 5% and  $A_{\perp}$  decreases from 21.6 to 20.0 Å<sup>2</sup>/molecule, when going from C14SH to C22SH. These  $A_{\perp}$  values are much larger than the herringbone-ordered crystalline phases of alkanes which have molecular areas of 18.5–19.0 Å<sup>2</sup>/molecule.<sup>59</sup> Rather, these values are close to those of the rotator phases of alkanes which exhibit a degree of chain disorder.<sup>59</sup> The decrease observed here in  $A_{\perp}$  with increasing  $n$  suggests that the increased chain–chain interaction is increasingly able to compensate for the headgroup interactions, which would prefer a different spacing and therefore distort the unit cell. Similar large values of  $A_{\perp}$  have been observed for the alkyl chains of phospholipids.<sup>61</sup> In that case, the headgroups are bulky and the molecules tilt to preserve the close contact between the chains. For alkane thiols on mercury, the S–Hg–S motif may also be responsible for the poor packing of the chains.

**Table 7. Comparison of the Structural Parameters of the Standing-Up Phases of Alkyl Thiols on Mercury and on Gold<sup>a</sup>**

<i>n</i>	$A_{\text{Hg}}$ Å <sup>2</sup> /mol.	$A_{\perp\text{Hg}}$ Å <sup>2</sup> /mol.	$\varphi_{\text{Hg}}$ °	$A_{\text{Au}}$ Å <sup>2</sup> /mol.	$A_{\perp\text{Au}}$ Å <sup>2</sup> /mol.	$\varphi_{\text{Au}}$ °
14	23.3	21.6	22–24	21.7	18.2	33
18	23.2	20.7	27	21.7	18.6	31
22	22.6	20.0	28	21.7	18.8	30
18(hex)	20.3	20.3	0			

<sup>a</sup> All molecular areas were obtained from GID measurements. Note that C18SH exhibits both a tilted rectangular and an untilted hexagonal phase. PACS numbers: 68.18.-g,61.10.Kw,68.03.Cd,68.65.Ac

A comparison between the structures of the alkyl-thiol SAMs on gold and alkyl-thiol LMs on mercury is very instructive. The most important differences and their chain length dependence are summarized in Table 7. The differences in the structure stem from the differences in the order of the substrate: a long-range-ordered crystalline solid in the case of gold, and a short-range-ordered liquid in the case of mercury. Consequently, some of the features which depend more sensitively on a delicate balance between the various interactions in the system, are also different. These features include the lying-down phase which, on gold, is long-range ordered and commensurate with the gold lattice<sup>62</sup> while it is disordered on the liquid mercury surface. Another feature is the azimuthal direction of the tilt of the standing-up phases which is along a nonsymmetry direction with an azimuthal angle varying with chain length for gold<sup>11,63</sup> whereas it is a fixed, length-independent, nearest-neighbor direction on mercury. The tilt magnitude is 30–33° on gold, whereas it is 22–28° on mercury. Another significant difference is the molecular area of the unit cell, which is much larger for thiols on mercury, not just in the plane of the substrate but even more so in the plane perpendicular to the molecular long axis. While thiols on mercury, as well as on gold, seem to prefer being tilted, on mercury we detected also an untilted hexagonal phase, which is not observed on gold.

The present X-ray studies need to be extended to shorter alkyl thiols for which multilayers have been observed in previous measurements.<sup>44</sup> Another direction, already being pursued, are LMs of thiols of molecules other than linear chains, and in particular those containing conjugated aromatic rings,<sup>36,42</sup> which are currently under intense study as possible single-molecule electronic devices.<sup>6,11,64,65</sup>

**Acknowledgment.** Support to M.D. by the U.S.–Israel Binational Science Foundation, Jerusalem is gratefully acknowledged. B.N.L. is supported by U.S. DOE Contract No. DE-AC02-98CH10886.

LA0701430

(61) Kuzmenko, I.; Kaganer, V. M.; Leiserowitz, L. *Langmuir* **1998**, *14*, 3882.

(62) Camillone, N.; et al. *J. Chem. Phys.* **1994**, *101*, 11031.

(63) Fenter, P.; Eberhardt, A.; Liang, K. S.; Eisenberger, P. *J. Chem. Phys.* **1997**, *106*, 1600.

(64) Bumm, L. A.; et al. *Science* **1996**, *271*, 1705. Tour, J. M.; et al. *J. Am. Chem. Soc.* **1995**, *117*, 9529; Adlkofer, K.; et al. *J. Phys. Chem. B* **2003**, *107*, 11737.

(65) Maltezos, G.; Nortrup, R.; Jeon, S.; Zaumseil, J.; Rogers, J. A. *Appl. Phys. Lett.* **2003**, *10*, 2067.